Polymer 148 (2018) 382–389

Contents lists available at ScienceDirect

Polymer

journal homepage: www.elsevier.com/locate/polymer

Linkage effects of triphenylamine-based aromatic polymer electrets on electrical memory performance

Shun-Wen Cheng [a, 1], Yu-Hsin Chang Chien [b, 1], Teng-Yung Huang [a], Cheng-Liang Liu [b, *], Guey-Sheng Liou [a, **]

[a] Institute of Polymer Science and Engineering, National Taiwan University, Taipei, 10617, Taiwan
[b] Department of Chemical and Materials Engineering, National Central University, Taoyuan, 32001, Taiwan

ARTICLE INFO

Article history:
Received 4 May 2018
Received in revised form
8 June 2018
Accepted 12 June 2018
Available online 13 June 2018

Keywords:
Polymer electret
Memory
Organic field effect transistor

ABSTRACT

Here, we use polyimide (**PI**), polyether (**PE**) and polyester (**PET**) with diphenyl sulfonyl (**S**) moieties combined with triphenylamine (**TPA**) units to obtain three polymer electrets, **TPA-PIS**, **TPA-PES**, and **TPA-PETS**, respectively. The pentacene-based organic field effect transistor (OFET) memories with the charge-trapping polymer electrets layer were examined. The variation in linkages in the polymer backbone noticeably influences the energy structures and molecular polarity, and thus their memory properties were systematically characterized and compared. Volatile memory characteristics can be observed for all three polymer electrets-based memories. Among these, the **TPA-PIS** and **TPA-PETS** electret OFET memory devices exhibit ambipolar trapping behavior capable of storing holes and electrons, with a memory window (**MW**) of 32.4 ± 1.2 V and 21.7 ± 1.0 V, respectively, and a memory ratio of 10^4~10^6. Importantly, programming/erasing switching endurance for at least 100 cycles is achieved, allowing for tri-state memory storage. However, hole-only unipolar trapping of OFETs memory with the **TPA-PES** electret presents relatively slower charge detrapping phenomena and longer retention time ability due to the higher molecular dipole moment. Our comparative study demonstrates the important role of the linkage effect in aromatic polymers for developing polymer electret-based OFET memories.

1. Introduction

The memory cell is an electronic transistor that stores the charge, and it can be set to store a logic 1 (high conductance state) and reset to logic 0 (low conductance state). Traditional inorganic semiconductor transistors are now widely used in all kinds of memory devices. Organic field effect transistor (OFET) memories are seen as emerging/promising memory technology due to their advantages of a low-cost and easy production process, as well as being perfectly compatible with complementary integrated circuits [1–7]. The types of OFET memories are divided into floating-gate memories [8–21], ferroelectric memories [22–26] and polymer electret memories [27–51]. Among these, more interest has been focused on polymer electret memories, since their memory characteristics can be efficiently manipulated by the molecular structures and composition of polymer or composite electrets. Therefore, it is of great interest to provide a broad pool of polymer electret materials and to further understand the related charge storage abilities.

Polymeric electret materials are electrically charged dielectric polymers. The architecture of OFETs involves the use of one additional polymer electret layer as a memory device. An electrical field is applied between the gate and semiconducting channel to modulate the charge carrier distribution in the OFETs. The trapped charge in the chargeable polymer electret results in the change in threshold voltage (V_{th}) of the OFETs memory related to the programming and erasing states. Single component polymer (pendent polymer [27–40] and donor-acceptor polyimide [41–44]) and polymer composite [46–49] are the main materials that are used in polymer electret memories. The fabrication of a solution-processed polymer electret layer and its interface with the top organic semiconductors has an influence on the resulting thin film morphologies, as well as the relative energy of the frontier molecular orbitals for hole/electron trapping condition and stability. It is thus necessary to develop a structural design of polymer electret materials that can also maintain good film quality. Donor/acceptor

* Corresponding author.
** Corresponding author.
E-mail addresses: clliu@ncu.edu.tw (C.-L. Liu), gsliou@ntu.edu.tw (G.-S. Liou).
[1] These authors contributed equally to this work.

https://doi.org/10.1016/j.polymer.2018.06.040
0032-3861/

strength and the side-chain conjugated length of polymer electrets have been shown to impact the memory performance. However, the effects of the linkages which are directly tethered to the backbone of the polymer electret are not yet understood. The engineering of the chemical linkages connecting the donor/acceptor units has the potential to control the memory properties of the aromatic polymer electrets that are synthesized.

In this study, the effects of the type of linkages between the fixed triphenylamine (**TPA**) donor and biphenyl sulfone (**S**) acceptor on the memory performance were investigated by using polyimide (**PI**), polyether (**PE**) and polyester (**PETS**) as the model polymer electrets. Pentacene-based OFET memories with these three polymer electret layers were fabricated and characterized. We found that linkage moieties play a critical role in dictating the electronic properties of the polymer electret thin film. The pentacene/polymer electret interface energy barrier can determine the polarity of the charge trapping behaviors, whereas the molecular dipole moment of the polymer electret influences the charge transfer behavior and the related dissipation of the transferred charges. Our findings offer insights that can be used to produce better molecular designs for developing polymer electret materials for the use in OFET memories.

2. Experimental section

2.1. Materials

All the commercially available reagents were used without further purification unless otherwise stated. The reagents 4,4′-dihydroxyltriphenylamine, 4,4′-diaminotriphenylamine, 4,4′-sulfonyldibenzoyl chloride and 3,3′,4,4′-diphenylsulfone tetracarboxylic dianhydride were prepared according to the procedure in the literature [52,53]. The synthesis details and basic characterization of the three TPA-based aromatic polymer electrets (**TPA-PES**, **TPA-PETS** and **TPA-PIS**) are available in the supporting information.

2.2. Instrumental characterization

Fourier transform infrared (FT-IR) spectra were recorded on a PerkinElmer Spectrum 100 Model FT-IR spectrometer. ^{1}H NMR spectra were measured on a Bruker AVIII 400 MHz spectrometer. The inherent viscosities were determined at 0.5 g dL^{-1} concentration using Tamson TV-2000 viscometer at 30 °C. Gel permeation chromatographic (GPC) analysis was carried out on a Waters chromatography unit interfaced with a Waters 2410 refractive index detector. Two Waters 5 μm Styragel HR-2 and HR-4 columns (7.8 mm I. D. × 300 mm) were connected in series with NMP as the eluent at a flow rate of 0.5 mL min^{-1} at 40 °C and were calibrated with polystyrene standards. Thermogravimetric analysis (TGA) was conducted with a heating rate of 20 °C min^{-1} under the nitrogen atmosphere on TA SDT Q600. DSC analyses were performed on a Perkin Elmer Pyris 1 DSC at a scan rate of 10 °C min^{-1} in flowing nitrogen. Cyclic voltammetry (CV) was recorded on a CH Instruments 611 B electrochemical analyzer in acetonitrile containing tetrabutylammonium perchlorate (TBAP, 0.1 M) as supporting electrolyte at a scan rate of 100 mV cm^{-1}. Counter and working electrode were made of ITO and Pt wire, respectively, and the reference electrode was taken by using a homemade Ag/AgCl, KCl (sat.). UV–visible absorption was recorded on UV–visible spectrophotometer (Hitachi U-4100).

2.3. Device fabrication and measurement

OFET memories with the device configuration of top-contact bottom-gate (BGTC) were fabricated onto highly doped n-type Si wafers with a thermally grown 300 nm-thick SiO_2 dielectric layer. The substrates were subsequently cleaned by acetone and isopropanol and then treated with plasma. Polymer electret thin films were deposited by spin-coating DMAc solutions (50 mg ml^{-1}, filtered with a PTFE syringe filter), followed by thermal annealing at 150 °C for 30 min. The thickness of the resulting polymeric films was determined to be ~50 nm. 50 nm pentacene was thermally evaporated on the top of the polymer thin films at the deposition temperature of 90 °C at 10^{-6} torr. Finally, 50 nm gold was deposited as the source and drain contacts. The channel length (L) and width (W) of the resulting OFET memory device were 50 and 1000 μm, respectively. The electrical characteristics were measured with a Keithley 4200-SCS semiconductor parameter analyzer. All the device fabrication and measurement procedures were carried out inside a N_2-filled glovebox.

3. Results and discussion

The chemical structures of three aromatic polymer electret materials are shown in Fig. 1 and the detailed synthetic routes for polymers are described in Scheme S1. Polycondensation between TPA- and diphenyl sulfonyl-containing monomers, which were synthesized according to reports in the previous literature, gave three final targets of polyimide (**TPA-PIS**), polyether (**TPA-PES**) and polyester (**TPA-PETS**). The chemical structures of the synthesized polymers were verified by FT-IR (Fig. S1) and ^{1}H NMR (Fig. S2). All three polymers were sufficiently soluble in common organic solvents, including tetrahydrofuran (THF), chloroform and dimethylacetamide (DMAc). Gel permeation chromatography (GPC) was used to determine the polymers' molecular weights and dispersities. The number average molecular weights (M_n) and polydispersity indexes (PDI) were found to be 64.1 kDa and 2.06 for **TPA-PIS**, 26.0 kDa and 2.34 for **TPA-PES**, and 54.0 kDa and 2.18 for **TPA-PETS**, respectively, as summarized in Table S1. The thermal properties of three polymers (Table S2) were also evaluated by thermogravimetric analysis (TGA) and differential scanning calorimetry (DSC). The degradation temperatures determined at 5% weight loss for the three polymers are higher than 450 °C under nitrogen atmosphere, and a distinct thermal transition during the second heating trace of DSC measurement was observed at 296, 189 and 208 °C for **TPA-PIS**, **TPA-PES** and **TPA-PETS**, respectively. These results indicate that the incorporation of aromatic imide linkages in **TPA-PIS** leads to enhanced thermal properties. The optical absorbance spectra and cyclic voltammograms (CV) of three polymers in thin films are shown in Fig. 2 and Fig. 3a, respectively, and the relevant data are summarized in Table 1. The high energy spectra feature around 300 nm is assigned to the localized transition, whereas the low energy adjoining shoulder of the **TPA-PIS** film and broad absorption tail of broad absorption of the **TPA-PETS** film may be ascribed to the charge transfer (CT) interaction. The absorption of this CT transition band is red-shifted to the lower energy region as the stronger electron-withdrawing imides were linked between TPA and sulfonyl groups. The CV of the three polymers show the distinct quasi-reversible oxidation peak and one irreversible reduction. The HOMO/LUMO energy levels (E_{HOMO}/E_{LUMO}) of all the polymers were determined from the corresponding onset oxidation/reduction potential ($E^{ox}_{onset}/E^{red}_{onset}$), versus the half-wave potentials of Fc/Fc$^+$ redox couple [54]. The relative energies are summarized in Table 1 and Fig. 3b.

It is clearly observed that **TPA-PIS** shows deeper-lying HOMO and LUMO than the other two polymers. This indicates that the strong electron-withdrawing of the linkage moieties and CT strength can be substantially found in the following order: **TPA-PIS** > **TPA-PETS** > **TPA-PES**. The bandgaps of **TPA-PIS**, **TPA-PES**, and **TPA-PETS**

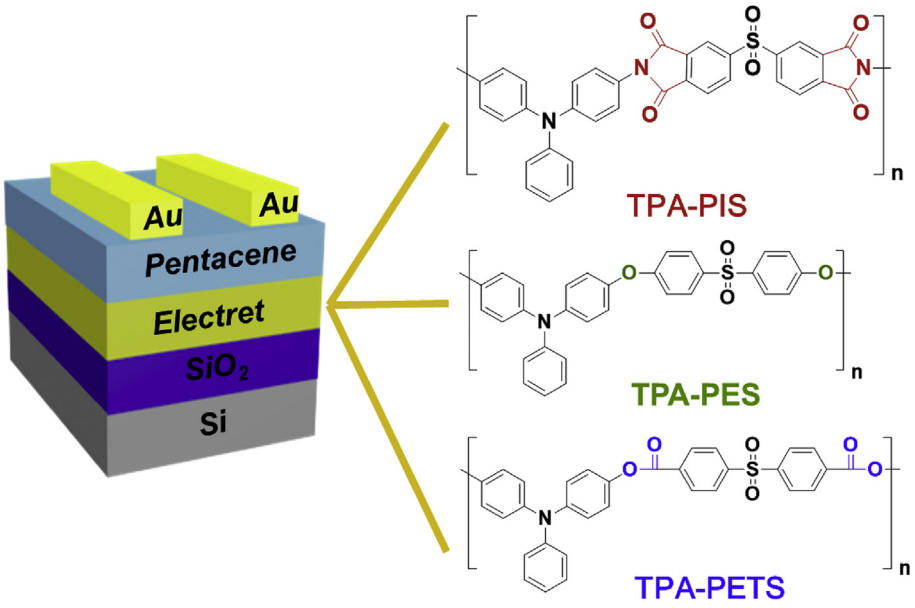

Fig. 1. Schematic configuration of OFET memory device and chemical structures of the polymer electret layers.

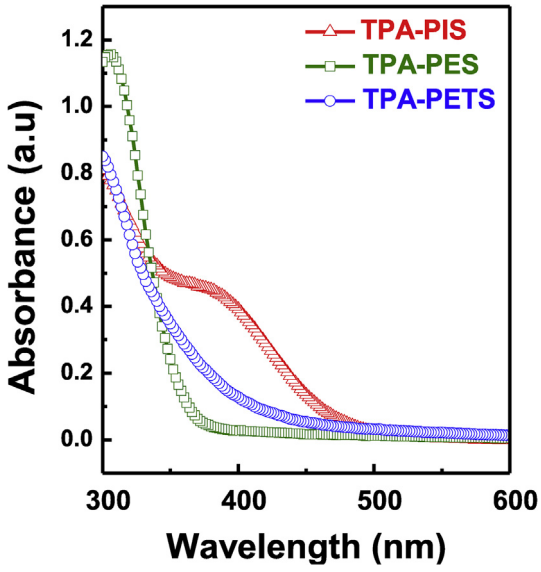

Fig. 2. UV–Vis absorption spectra of the spin-coated polymer film.

are estimated to be 2.20, 2.89 and 2.60 eV, respectively, derived from the difference between their HOMOs and LUMOs. DFT calculation at the B3LYP/6-31G(d) model with the Gaussian 09 program was performed to investigate the optimized molecular conformation and electronic structure, in which the polymer structures were represented by monomeric units in order to simplify the calculations. The estimated frontier molecular orbitals of the model molecules are shown in Fig. S3. The HOMO and LUMO are relatively localized at the TPA donor backbone and sulfone (or imide for **TPA-PIS**) accepter core, respectively. The same trend in energy levels was observed between the computational study and experimental results mentioned above. The progressive decreases in both the electrochemical bandgap and HOMO energy level are mainly due to the strong imide acceptors that are covalently linked. It is primarily concluded that the change in linkage groups in the structures of polymer electrets plays an important role in the electronic properties and their corresponding memory device performance.

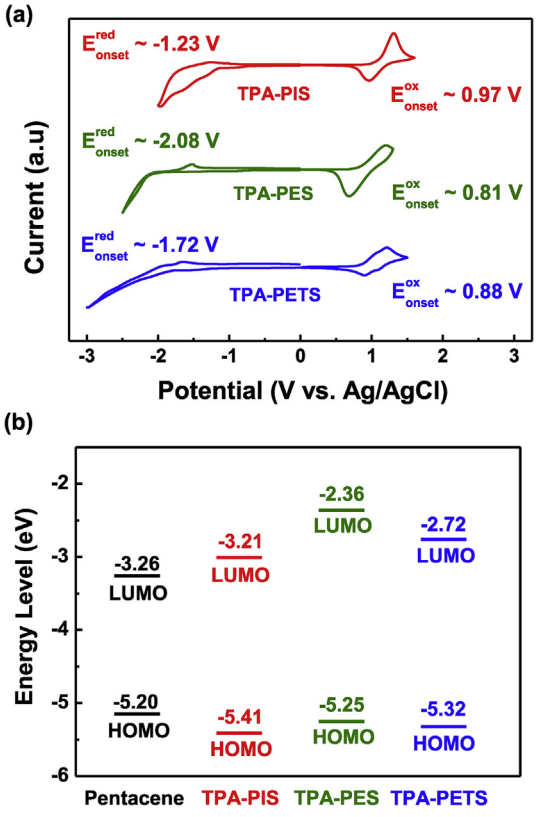

Fig. 3. (a) Cyclic voltammograms and (b) relative electrochemical energy levels of the polymer electret and pentacene.

Spin-coating from the polymer solutions provides a ~50 nm thick dry polymer electret film which forms smooth trapping layers with good surface quality and contact angle uniformity. Our results confirm that the polymer surface is slightly hydrophobic judging from the water contact angle measurement (~80°, Fig. S4), and is smooth and pinhole-free in the AFM analysis (root-mean-square roughness (R_{RMS}) < 0.5 nm; Fig. 4a and c). Therefore, the

Table 1
Optical and electrochemical properties of the synthesized polymers.

Polymer	λ^{a}_{onset} (nm)	E^{ox}_{onset} [b] (V)	E^{red}_{onset} [c] (V)	E^{d}_{HOMO} (eV)	E^{d}_{LUM} (eV)	E^{e}_{g} (eV)
TPA-PIS	517	0.97	−1.23	−5.41	−3.21	2.20
TPA-PES	409	0.81	−2.08	−5.25	−2.36	2.89
TPA-PETS	484	0.88	−1.72	−5.32	−2.73	2.60

[a] Absorbance onset measured in thin film.
Onset potential vs Ag/AgCl in [b] CH_3CN and [c] DMF.
[d] HOMO and LUMO energy levels were calculated from formula $E_{HOMO} = -(4.44 + E^{ox}_{onset})$ and $E_{LUMO} = -(4.44 + E^{red}_{onset})$.
[e] $Eg = -(E_{HOMO}-E_{LUMO})$.

featureless and non-polar polymer electret/SiO_2 surface considerably favors the diffusion of pentacene molecules as well as the coalescence of grains to form large island-like domains, as shown in Fig. 4d and f.

Fig. 1 shows the schematic configuration of the fabricated BGTC OFET memories with three different polymer charge trapping electret layers. The electrical transfer characteristics of the polymer electret-based OFET memories were measured by applying various bidirectional gate voltages (V_g). The field effect mobility (μ) of each transistor was calculated from the saturated region (drain voltage (V_d) of −100 V) with the following equation (1):

$$I_d = \frac{W}{2L} C_{total} \mu (V_g - V_{th})^2 \quad (1)$$

where I_d and V_{th} are drain current and threshold voltage, respectively. The total areal capacitance (C_{total}) of the dielectric containing polymer electret and SiO_2 bilayer in series was obtained from equation (2), where C_{PE} and C_{ox} are the areal capacitance of the polymer electret (with respective to frequency of 10 kHz) and oxide, respectively.

$$\frac{1}{C_{total}} = \frac{1}{C_{PE}} + \frac{1}{C_{OX}}. \quad (2)$$

The extracted hole mobility of these OFETs is approximately in the range of 0.10–0.27 $cm^2 V^{-1} s^{-1}$. The ON/OFF ratio (I_{ON}/I_{OFF}) of OFETs is greater than 10^6. The electrical characteristics of OFETs are summarized in Table 2. Uniform performance in OFETs with three different polymer electrets was achieved with reasonably good mobility, which is likely attributed to the large connected pentacene islands. It is noted that all these mobility values are almost always in this order of magnitude, no matter how the V_g sweeping ranges after applying the V_g bias vary.

The transfer characteristics under the V_g bias were further explored to demonstrate the storage capability of polymer electret-based OFET memory (Fig. 5). The amount of charge storage in the polymer electret layer can be modulated by changing the positive and negative voltage applied on the bottom gate. It should be noted that electrical memory operation conducted here is through consecutive V_g pulse measurement. The initial curves (black line in Fig. 5) of the three memory devices were measured with V_g sweeping from 20 to −40 V at V_d of −100 V. As shown in Fig. 5a for **TPA-PIS** and Fig. 5c for **TPA-PETS**, respectively, the transfer curve shifts obviously from the initial position toward the positive direction (route (i)) and negative position (route (iii)) after the 100 V and −100 V V_g are supplied for 15 s, respectively, reflecting the combined effect caused by the electron and hole trapping (or so-

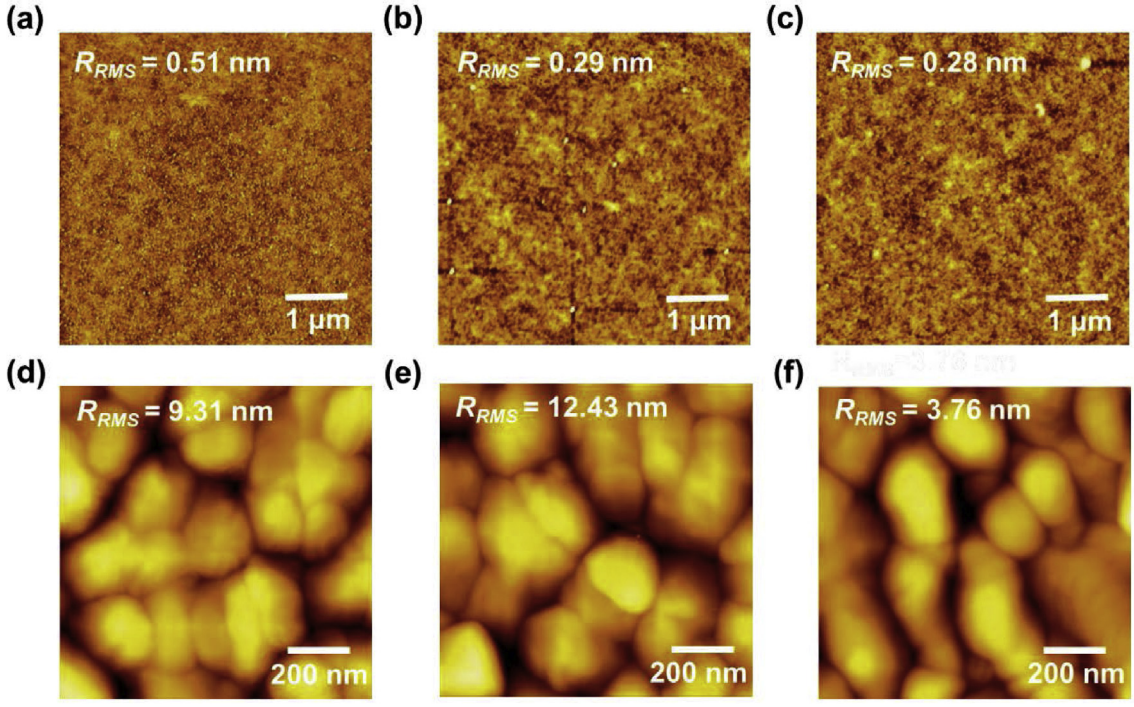

Fig. 4. AFM topographic images of electret films of (a) **TPA-PIS**, (b) **TPA-PES** and (c) **TPA-PETS**. AFM topographic images of thermal evaporated pentacene on top of the electret films of (d) **TPA-PIS**, (e) **TPA-PES** and (f) **TPA-PETS**.

Table 2
Memory properties of OFET memory with three polymer electret materials.

Polymer	M ($cm^2\ V^{-1}\ s^{-1}$)	MW (V)	MW^e (V)	MW^h (V)	Memory ratio (−)
TPA-PIS	0.27 ± 0.05	32.4 ± 1.2	13.4 ± 1.2	19.0 ± 0.7	10^5–10^6
TPA-PES	0.22 ± 0.01	43.2 ± 4.7	–	43.2 ± 4.7	10^5–10^6
TPA-PETS	0.10 ± 0.04	21.7 ± 1.0	9.2 ± 1.3	12.5 ± 1.4	10^3–10^4

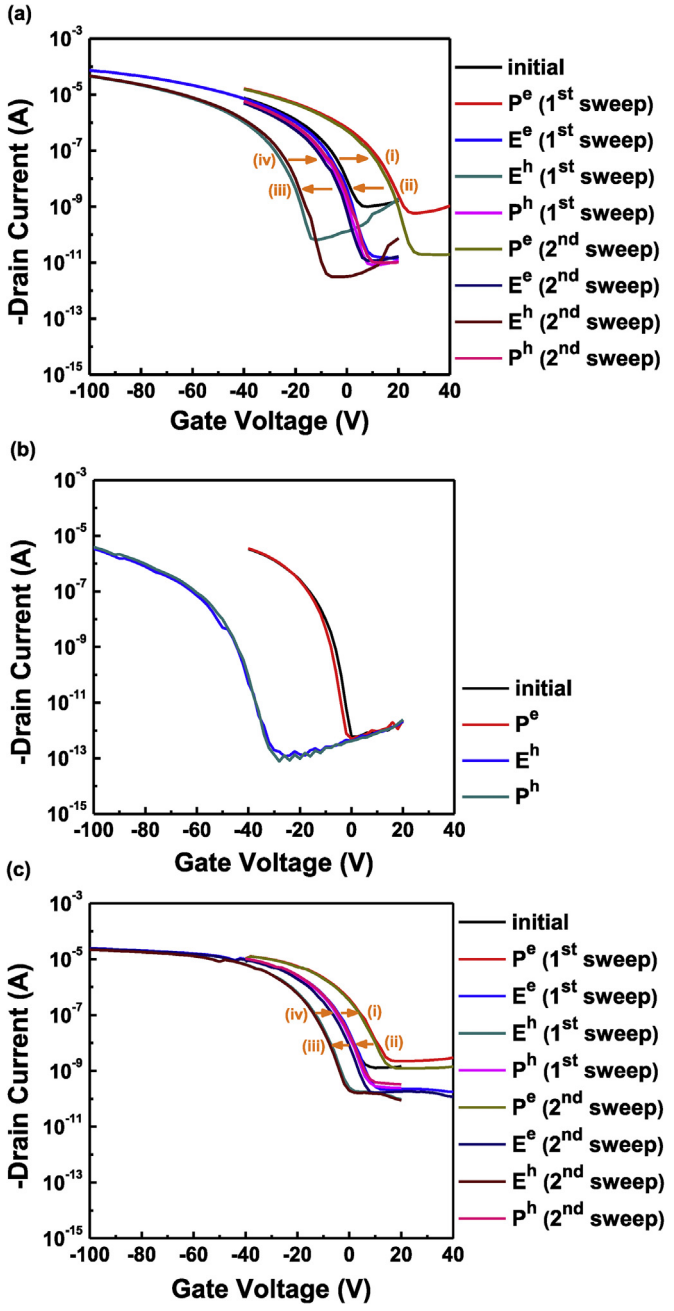

Fig. 5. Transfer characteristics of OFET memories based on (a) **TPA-PIS**, (b) **TPA-PES** and (c) **TPA-PETS** electret under the programming and erasing operation, where P^e: $V_g = 100$ V, 15 s; E^e: $V_g = -100$ V, 5 s; E^h: $V_g = -100$ V, 15 s; P^h: $V_g = 100$ V, 5 s and V_d in all the measurements is fixed at −100 V.

called ambipolar trapping) ability. As a result, these two OFET memories exhibit ambipolar charge trapping, where the trapped charge carriers, electrons and holes can module the I_d, as evidenced by the electron programming (P^e) state and hole erasing (E^h) state, respectively, relative to the initial state [16,17,19,49]. It should be noted here that the positive/negative shift corresponds to the programming (P) and erasing (E) operation. The negatively (route (ii)) and positively (route (iv)) shifted transfer curve returns back to the initial curve after the opposite polarity of V_g is applied for 5 s, and this is assigned to the electron erasing (E^e) state and hole programming (P^h) state, respectively. Additionally, similar routes of shifts in the transfer curve can be programmable/erasable for the second sweep. The memory window (MW) is calculated from the sum of the shift of V_{th} in the transfer curves between the P^e and initial state (MW^e; from trapped electrons) and between the E^h and initial state (MW^h; from trapped holes). Since the memory operation in **TPA-PIS** and **TPA-PETS** electret-based OFET memory is highly reliable, the MW is averaged out of 10 devices in one batch. The MW thus obtained is 32.4 ± 1.2 V and 21.7 ± 1.0 V for **TPA-PIS** and **TPA-PETS**, respectively. The memory ratio, defined by the ratio between the high and low I_d at V_g of −5 V (reading at P^e and E^h state, respectively), is 10^4~10^6. The memory results mentioned above are summarized in Table 2. On the other hand, the transfer curve only shifts towards the negative direction from the initial curve after E^h operation (no positive shift after P^e process) for the OFET memory device with the **TPA-PES** electret layer (Fig. 5b), suggesting the positive charges are stored in the **TPA-PES** electret or pentacene/**TPA-PES** interlayer to impede the accumulation of hole channels. However, the negatively shifted transfer curve after P^h operation does not return to the initial state. The MW of the device with the **TPA-PES** electret is calculated to be 43.2 ± 4.7 V, which can be a clear signal of a large amount of hole trapping. This unipolar trapping behavior is mainly due to the large potential barrier of 0.9 eV from the difference between the LUMO of **TPA-PES** electret and pentacene, which serves to deplete the electron movement upon the P^e process [20,21]. Although the control V_g is quite high (−100 V) and the applied voltage pulse is quite wide (5 or 15 s) for present polymer electret-based OFET memories, these parameters can be modified after optimizing the device geometry, such as the oxide thickness.

To demonstrate further the stability of the device, the transfer curves after E^h process are steadily measured over a fixed period of time. It is emphasized that the V_g is not further biased during the test; in other words, the power is interrupted. As shown in Fig. 6, an initial transfer curve of **TPA-PES** electret-based OFET memory is first recorded and has an obvious negative V_{th} shift after E^h process. After that, the subsequent measurements show that the transfer curve can be only retained temporarily. The shifting in transfer curve toward the positive side starting from 1 min and finally close to the initial one after 150 min. This electrical relaxation is a proof-of-principle demonstration of volatile memory functionality in our device. Similar relaxation behavior in electrical transfer characteristics can be also observed in the volatile **TPA-PIS** and **TPA-PETS** electret-based OFET memories (Fig. S5 and S6). Due to their ambipolar charge trapping phenomena, the transfer curves after E^h (Fig. S5a and S6a of Supporting Information) and P^e process (Fig. S5b and S6b) are shifted in the positive and negative voltage direction, respectively, upon the removal of the V_g. Comparatively, the charge trapping state of OFET devices based on these two polymer electrets is not stable relative to device based on **TPA-PES** electret since the transfer curve is quickly shifted back to the initial condition within few minutes. It should be concluded here that all

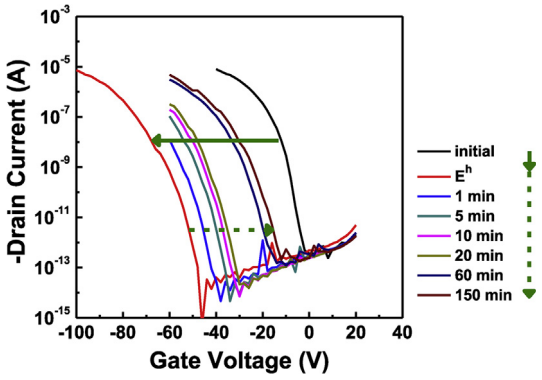

Fig. 6. Transfer characteristics of **TPA-PES** electret-based OFET memories in the initial condition, E^h process ($V_g = -100$ V, 15 s) and various conditions for 1–150 min after removal of negative V_g bias.

three aromatic polymer electrets-based OFET devices exhibit the volatile memory nature and the reason for influencing the underlying memory performance will be discussed latter.

To investigate the tunability of the OFET devices under different V_g, the dynamic behavior of devices based on **TPA-PIS** and **TPA-PETS** electrets was tested for memory cyclic endurance (Fig. 7). Under a fixed V_d of −100 V, switching between the tristable states is achieved using sequential V_g application for P^e, E^e, E^h, and P^h operation. A positive (P^e operation)/negative (E^h operation) voltage bias applied for long enough time will induce electron/hole accumulation and transfer the charges into the trapped sites, which causes a positive (negative) V_{th} shift. On the other hand, the stored electron/hole can be detrapped by applying the V_g in the opposite polarity for E^e/P^h operation, and both the extracted V_{th} values become intermediate and almost overlap. These results indicate the OFET memory with the **TPA-PIS** or **TPA-PETS** electret maintains a substantial window margin even after 100 cycles of operation. Electrical switching between these three distinguished states realized by modulating the applied V_g bias is important for overcoming the limitation of the low-density storage of digital memory.

The retention ability between the high current state, initial state and low current state was measured at a constant V_g of −5 V (Fig. 8).

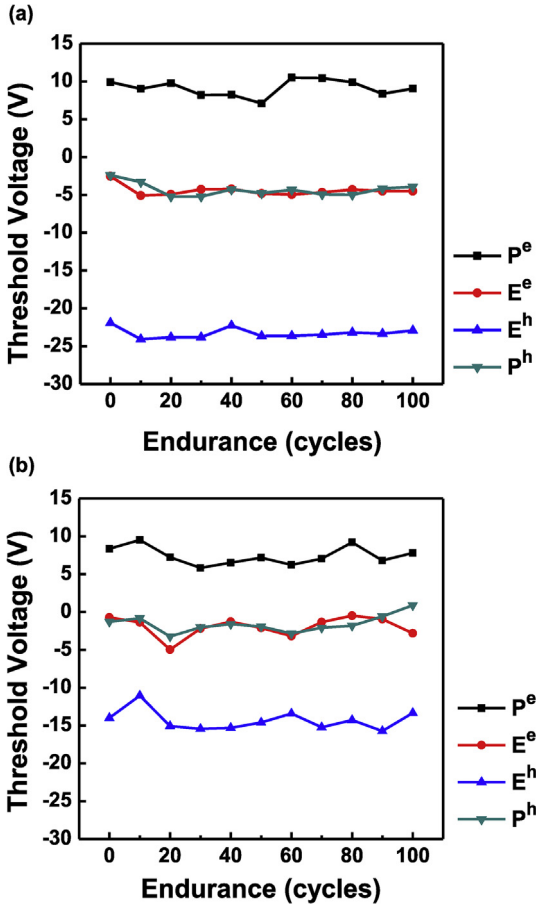

Fig. 7. Cyclic endurance characteristics of OFET memories based on (a) **TPA-PIS** and (b) **TPA-PETS** electrets, where P^e: $V_g = 100$ V, 15 s; E^e: $V_g = -100$ V, 5 s; E^h: $V_g = -100$ V, 15 s; P^h: $V_g = 100$ V, 5 s and V_d in all the measurements is fixed at −100 V.

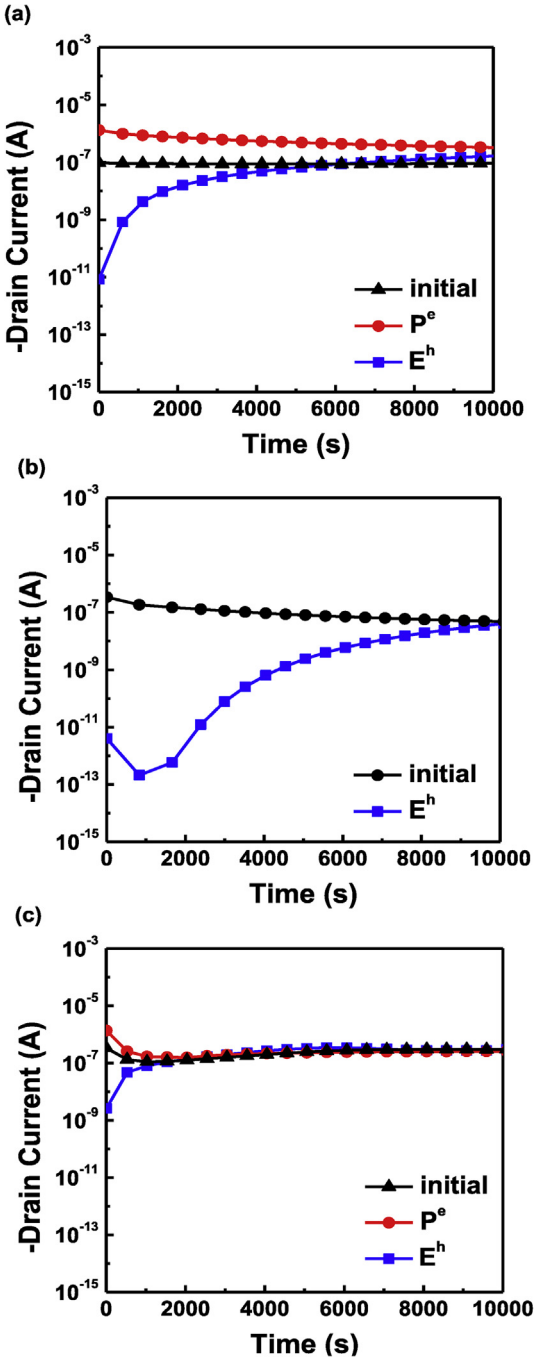

Fig. 8. The data retention characteristics of OFET memories based on (a) **TPA-PIS**, (b) **TPA-PES** and (c) **TPA-PETS** electrets, where P^e: $V_g = 100$ V, 15 s and E^h: $V_g = -100$ V, 15 s and the reading V_g and V_d are fixed at −5 V and −100 V, respectively.

One interesting phenomenon that occurred is that the low current state after E_h operation in all three devices gradually returns to the initial state due to the loss in stored hole. Leakage pathways through the blocking dielectric/polymer electret layer can be excluded from this process, since the smooth bilayer-surface reduces this type of charge dissipation. Although the detailed charge relaxation mechanism is not fully understood, we think that the memory switching behavior can be explained by electrical field-induced charge trapping in the electret. The short charge retention time can probably be attributed to the small barrier offset between the HOMO levels of the polymer electret and semiconducting pentacene. Similar electrical characteristics for the decay in the high current state can be detected for the **TPA-PIS** or **TPA-PETS** electret devices due to the electron detrapping. These three polymer electrets-based OFET memory devices have volatile memory, since all lose their information if they lose the power. The time period of charge confinement in the trapping sites may be determined from the polarity of the polymer electret materials. The molecular dipole was also theoretically calculated from the DFT ground state optimized molecular geometries. Very large differences in dipole moments were obtained by changing the linkage groups in these three polymer electrets. The model compound calculations yield a dipole moment of 3.93, 6.01 and 5.49 Debye for the **TPA-PIS**, **TPA-PES** and **TPA-PETS** electrets, respectively. High molecular dipole species in the **TPA-PES** electret may stabilize the radical cation and sustain the charge storage more efficiently [43]. Therefore, OFET memory with the **TPA-PES** electret shows relatively slower charge depletion and longer retention as compared to the other two electrets.

4. Conclusions

In summary, we have successfully synthesized a series of aromatic polymer electret containing the **TPA** and sulfonyl (**S**) backbone and investigated the effects of the linkages on the memory performance of OFET memory devices. The linkage moieties, imide (**I**), ether (**E**) and ester (**ET**), have a substantial effect on governing the optical, structural and memory data of the resulting polymer electret. OFET memories with pentacene semiconductor and **TPA-PIS** and **TPA-PETS** electret layers exhibit ambipolar charge trapping behavior, and thus the V_{th} shifts in both positive and negative directions expand the memory window of 32.4 ± 1.2 and 21.7 ± 1.0 V, respectively. However, unipolar hole trapping can be detected in the **TPA-PES** device due to the high-lying LUMO level of the trapping electret and its large barrier offset with pentacene. Although volatile characteristics are observed for all three devices, the **TPA-PES** electret-based device still exhibits a relatively slower charge detrapping behavior and longer retention ability, mainly due to the higher calculated dipole moment. This study demonstrates that incorporation of different linkages into the backbone of the aromatic polymer electret can further manipulate the memory performance.

Acknowledgements

This work was financially supported by the Advanced Research Center of Green Materials Science and Technology from The Featured Area Research Center Program within the framework of the Higher Education Sprout Project by the Ministry of Education (107L9006) and the Ministry of Science and Technology in Taiwan (107-3017-F-002-001, 105-2628-E-008-008-MY3, and 104-2113-M-002-002-MY3).

Appendix A. Supplementary data

Supplementary data related to this article can be found at https://doi.org/10.1016/j.polymer.2018.06.040.

References

[1] Q.-D. Ling, D.-J. Liaw, C. Zhu, D.S.-H. Chan, E.-T. Kang, K.-G. Neoh, Polymer electronic memories: materials, devices and mechanisms, Prog. Polym. Sci. 33 (2008) 917–978.
[2] Y. Guo, G. Yu, Y. Liu, Functional organic field-effect transistors, Adv. Mater. 22 (2010) 4427–4447.
[3] P. Heremans, G.H. Gelinck, R. Muller, K.-J. Baeg, D.-Y. Kim, Y.-Y. Noh, Polymer and organic nonvolatile memory devices, Chem. Mater. 23 (2010) 341–358.
[4] B.M. Dhar, R. Özgün, T. Dawidczyk, A. Andreou, H.E. Katz, Threshold voltage shifting for memory and tuning in printed transistor circuits, Mater. Sci. Eng. R Rep. 72 (2011) 49–80.
[5] S.T. Han, Y. Zhou, V. Roy, Towards the development of flexible non-volatile memories, Adv. Mater. 25 (2013) 5425–5449.
[6] Y.-H. Chou, H.-C. Chang, C.-L. Liu, W.-C. Chen, Polymeric charge storage electrets for non-volatile organic field effect transistor memory devices, Polym. Chem. 6 (2015) 341–352.
[7] C.-C. Shih, W.-Y. Lee, W.-C. Chen, Nanostructured materials for non-volatile organic transistor memory applications, Mater. Horiz. 3 (2016) 294–308.
[8] T. Sekitani, T. Yokota, U. Zschieschang, H. Klauk, S. Bauer, K. Takeuchi, M. Takamiya, T. Sakurai, T. Someya, Organic nonvolatile memory transistors for flexible sensor arrays, Science 326 (2009) 1516–1519.
[9] S.-T. Han, Y. Zhou, Q.D. Yang, L. Zhou, L.-B. Huang, Y. Yan, C.-S. Lee, V.A. Roy, Energy-band engineering for tunable memory characteristics through controlled doping of reduced graphene oxide, ACS Nano 8 (2014) 1923–1931.
[10] S.T. Han, Y. Zhou, C. Wang, L. He, W. Zhang, V. Roy, Layer-by-layer-assembled reduced graphene oxide/gold nanoparticle hybrid double-floating-gate structure for low-voltage flexible flash memory, Adv. Mater. 25 (2013) 872–877.
[11] C.-W. Tseng, Y.-T. Tao, Electric bistability in pentacene film-based transistor embedding gold nanoparticles, J. Am. Chem. Soc. 131 (2009) 12441–12450.
[12] C.-W. Tseng, D.-C. Huang, Y.-T. Tao, Azobenzene-functionalized gold nanoparticles as hybrid double-floating-gate in pentacene thin-film transistors/memories with enhanced response, retention, and memory windows, ACS Appl. Mater. Interfaces 5 (2013) 9528–9536.
[13] C.-W. Tseng, D.-C. Huang, Y.-T. Tao, Electric bistability induced by incorporating self-assembled monolayers/aggregated clusters of azobenzene derivatives in pentacene-based thin-film transistors, ACS Appl. Mater. Interfaces 4 (2012) 5483–5491.
[14] R.H. Kim, J. Lee, K.L. Kim, S.M. Cho, D.H. Kim, C. Park, Flexible nonvolatile transistor memory with solution-processed transition metal dichalcogenides, Small 13 (2017), 1603971.
[15] X. Gao, X.-J. She, C.-H. Liu, Q.-J. Sun, J. Liu, S.-D. Wang, Organic field-effect transistor nonvolatile memories based on hybrid nano-floating-gate, Appl. Phys. Lett. 102 (2013), 023303.
[16] H.C. Chang, C. Lu, C.L. Liu, W.C. Chen, Single-crystal C60 needle/CuPc nanoparticle double floating-gate for low-voltage organic transistors based nonvolatile memory devices, Adv. Mater. 27 (2015) 27–33.
[17] Y. Zhou, S.T. Han, Z.X. Xu, V. Roy, Controlled ambipolar charge transport through a self-assembled gold nanoparticle monolayer, Adv. Mater. 24 (2012) 1247–1251.
[18] Y. Zhou, S.-T. Han, Y. Yan, L.-B. Huang, L. Zhou, J. Huang, V. Roy, Solution processed molecular floating gate for flexible flash memories, Sci. Rep. 3 (2013) 3093.
[19] Y. Zhou, S.-T. Han, P. Sonar, V. Roy, Nonvolatile multilevel data storage memory device from controlled ambipolar charge trapping mechanism, Sci. Rep. 3 (2013) 2319.
[20] M. Kang, K.J. Baeg, D. Khim, Y.Y. Noh, D.Y. Kim, Printed, flexible, organic nano-floating-gate memory: effects of metal nanoparticles and blocking dielectrics on memory characteristics, Adv. Funct. Mater. 23 (2013) 3503–3512.
[21] M. Kang, D. Khim, W.-T. Park, J. Kim, J. Kim, Y.-Y. Noh, K.-J. Baeg, D.-Y. Kim, Synergistic high charge-storage capacity for multi-level flexible organic flash memory, Sci. Rep. 5 (2015), 12299.
[22] R.H. Kim, H.J. Kim, I. Bae, S.K. Hwang, D.B. Velusamy, S.M. Cho, K. Takaishi, T. Muto, D. Hashizume, M. Uchiyama, Non-volatile organic memory with sub-millimetre bending radius, Nat. Commun. 5 (2014) 3583.
[23] S.-W. Jung, J.B. Koo, C.W. Park, B.S. Na, N.-M. Park, J.-Y. Oh, Y.G. Moon, S.S. Lee, K.-W. Koo, Non-volatile organic ferroelectric memory transistors fabricated using rigid polyimide islands on an elastomer substrate, J. Mater. Chem. C 4 (2016) 4485–4490.
[24] S.J. Kang, I. Bae, Y.J. Park, T.H. Park, J. Sung, S.C. Yoon, K.H. Kim, D.H. Choi, C. Park, Non-volatile ferroelectric poly (vinylidene fluoride-co-trifluoroethylene) memory based on a single-crystalline tri-iso-propylsilylethynyl pentacene field-effect transistor, Adv. Funct. Mater. 19 (2009) 1609–1616.
[25] S.J. Kang, Y.J. Park, I. Bae, K.J. Kim, H.C. Kim, S. Bauer, E.L. Thomas, C. Park, Printable ferroelectric PVDF/PMMA blend films with ultralow roughness for low voltage non-volatile polymer memory, Adv. Funct. Mater. 19 (2009)

2812–2818.
[26] S.J. Kang, I. Bae, Y.J. Shin, Y.J. Park, J. Huh, S.-M. Park, H.-C. Kim, C. Park, Nonvolatile polymer memory with nanoconfinement of ferroelectric crystals, Nano Lett. 11 (2010) 138–144.
[27] K.J. Baeg, Y.Y. Noh, J. Ghim, S.J. Kang, H. Lee, D.Y. Kim, Organic non-volatile memory based on pentacene field-effect transistors using a polymeric gate electret, Adv. Mater. 18 (2006) 3179–3183.
[28] K.J. Baeg, Y.Y. Noh, J. Ghim, B. Lim, D.Y. Kim, Polarity effects of polymer gate electrets on non-volatile organic field-effect transistor memory, Adv. Funct. Mater. 18 (2008) 3678–3685.
[29] Y. Guo, C.a. Di, S. Ye, X. Sun, J. Zheng, Y. Wen, W. Wu, G. Yu, Y. Liu, Multibit storage of organic thin-film field-effect transistors, Adv. Mater. 21 (2009) 1954–1959.
[30] J.-C. Hsu, W.-Y. Lee, H.-C. Wu, K. Sugiyama, A. Hirao, W.-C. Chen, Nonvolatile memory based on pentacene organic field-effect transistors with polystyrene para-substituted oligofluorene pendent moieties as polymer electrets, J. Mater. Chem. 22 (2012) 5820–5827.
[31] K.J. Baeg, D. Khim, J. Kim, B.D. Yang, M. Kang, S.W. Jung, I.K. You, D.Y. Kim, Y.Y. Noh, High-performance top-gated organic field-effect transistor memory using electrets for monolithic printed flexible NAND flash memory, Adv. Funct. Mater. 22 (2012) 2915–2926.
[32] X.-J. She, J. Liu, J.-Y. Zhang, X. Gao, S.-D. Wang, Spatial profile of charge storage in organic field-effect transistor nonvolatile memory using polymer electret, Appl. Phys. Lett. 103 (2013), 143302.
[33] Y.-C. Chiu, C.-L. Liu, W.-Y. Lee, Y. Chen, T. Kakuchi, W.-C. Chen, Multilevel nonvolatile transistor memories using a star-shaped poly ((4-diphenylamino) benzyl methacrylate) gate electret, NPG Asia Mater. 5 (2013) e35.
[34] Y.-H. Chou, S. Takasugi, R. Goseki, T. Ishizone, W.-C. Chen, Nonvolatile organic field-effect transistor memory devices using polymer electrets with different thiophene chain lengths, Polym. Chem. 5 (2014) 1063–1071.
[35] H.-S. Sun, Y.-C. Chiu, W.-Y. Lee, Y. Chen, A. Hirao, T. Satoh, T. Kakuchi, W.-C. Chen, Synthesis of oligosaccharide-based block copolymers with pendent π-conjugated oligofluorene moieties and their electrical device applications, Macromolecules 48 (2015) 3907–3917.
[36] S. Nam, J. Seo, H. Kim, Y. Kim, 5 V driving organic non-volatile memory transistors with poly (vinyl alcohol) gate insulator and poly (3-hexylthiophene) channel layers, Appl. Phys. Lett. 107 (2015), 153302.
[37] F.J. Chung, H.Y. Liu, B.Y. Jiang, G.Y. He, S.H. Wang, W.C. Wu, C.L. Liu, Random styrenic copolymers with pendant pyrene moieties: synthesis and applications in organic field-effect transistor memory, J. Polym. Sci. Polym. Chem. 54 (2016) 910–917.
[38] C.-T. Lo, Y. Watanabe, H. Oya, K. Nakabayashi, H. Mori, W.-C. Chen, Non-volatile transistor memory devices using charge storage cross-linked core–shell nanoparticles, Chem. Commun. 52 (2016) 7269–7272.
[39] J. Seo, S. Nam, H. Kim, T.D. Anthopoulos, D.D. Bradley, Y. Kim, Strong molecular weight effects of gate-insulating memory polymers in low-voltage organic nonvolatile memory transistors with outstanding retention characteristics, NPG Asia Mater. 8 (2016) e235.
[40] C. Lee, J. Seo, J. Kim, J. Jeong, H. Han, H. Kim, Y. Kim, Polymer nanodot-hybridized alkyl silicon oxide nanostructures for organic memory transistors with outstanding high-temperature operation stability, Sci. Rep. 6 (2016), 33863.
[41] Y.-H. Chou, N.-H. You, T. Kurosawa, W.-Y. Lee, T. Higashihara, M. Ueda, W.-C. Chen, Thiophene and selenophene donor–acceptor polyimides as polymer electrets for nonvolatile transistor memory devices, Macromolecules 45 (2012) 6946–6956.
[42] Y.-H. Chou, H.-J. Yen, C.-L. Tsai, W.-Y. Lee, G.-S. Liou, W.-C. Chen, Nonvolatile transistor memory devices using high dielectric constant polyimide electrets, J. Mater. Chem. C 1 (2013) 3235–3243.
[43] A.D. Yu, T. Kurosawa, M. Ueda, W.C. Chen, Polycyclic arene-based D–A polyimide electrets for high-performance n-type organic field effect transistor memory devices, J. Polym. Sci. Polym. Chem. 52 (2014) 139–147.
[44] L. Dong, H.S. Sun, J.T. Wang, W.Y. Lee, W.C. Chen, Fluorene based donor-acceptor polymer electrets for nonvolatile organic transistor memory device applications, J. Polym. Sci. Polym. Chem. 53 (2015) 602–614.
[45] H. Ling, J. Lin, M. Yi, B. Liu, W. Li, Z. Lin, L. Xie, Y. Bao, F. Guo, W. Huang, Synergistic effects of self-doped nanostructures as charge trapping elements in organic field effect transistor memory, ACS Appl. Mater. Interfaces 8 (2016) 18969–18977.
[46] Y.-C. Chiu, T.-Y. Chen, Y. Chen, T. Satoh, T. Kakuchi, W.-C. Chen, High-performance nonvolatile organic transistor memory devices using the electrets of semiconducting blends, ACS Appl. Mater. Interfaces 6 (2014) 12780–12788.
[47] Y.C. Chiu, I. Otsuka, S. Halila, R. Borsali, W.C. Chen, High-Performance nonvolatile transistor pemories of pentacence using the green electrets of sugar-based block copolymers and their supramolecules, Adv. Funct. Mater. 24 (2014) 4240–4249.
[48] Y.-H. Chou, Y.-C. Chiu, W.-Y. Lee, W.-C. Chen, Non-volatile organic transistor memory devices using the poly (4-vinylpyridine)-based supramolecular electrets, Chem. Commun. 51 (2015) 2562–2564.
[49] H.-Y. Chi, H.-W. Hsu, S.-H. Tung, C.-L. Liu, Nonvolatile organic field-effect transistors memory devices using supramolecular block copolymer/functional small molecule nanocomposite electret, ACS Appl. Mater. Interfaces 7 (2015) 5663–5673.
[50] J. Lin, W. Li, Z. Yu, M. Yi, H. Ling, L. Xie, S. Li, W. Huang, π-Conjugation-interrupted hyperbranched polymer electrets for organic nonvolatile transistor memory devices, J. Mater. Chem. C 2 (2014) 3738–3743.
[51] Y.C. Chiu, H.S. Sun, W.Y. Lee, S. Halila, R. Borsali, W.C. Chen, Oligosaccharide carbohydrate dielectrics toward high-performance non-volatile transistor memory devices, Adv. Mater. 27 (2015) 6257–6264.
[52] C.-J. Chen, Y.-C. Hu, G.-S. Liou, Linkage effect on the memory behavior of sulfonyl-containing aromatic polyether, polyester, polyamide, and polyimide, Chem. Commun. 49 (2013) 2536–2538.
[53] C.J. CHen, H.J. Yen, W.C. Chen, G.S. Liou, Novel high-performance polymer memory devices containing (OMe) 2tetraphenyl-p-phenylenediamine moieties, J. Polym. Sci. Polym. Chem. 49 (2011) 3709–3718.
[54] H.-C. Wu, C.-L. Liu, W.-C. Chen, Donor–acceptor conjugated polymers of arylene vinylene with pendent phenanthro [9, 10-d] imidazole for high-performance flexible resistor-type memory applications, Polym. Chem. 4 (2013) 5261–5269.